

Dimer-covering resonating-valence-bond treatment of single-walled zigzag carbon nanotubes

M.A. Garcia-Bach

Departament de Física Fonamental, Facultat de Física and Institut de Química Teòrica i Computacional, Universitat de Barcelona, Diagonal 647, 08028-Barcelona, Catalonia, Spain.

e-mail: m.angels.garcia.bach@ub.edu

Received: February 18, 2011/ Revised version: date

Abstract. Single-walled zigzag carbon nanotubes with h hexagons around the carbon nanotube, h ranging from 3 to 19, have been investigated from a resonating-valence-bond point of view. The energies calculated for the undoped $h = 3n - 1$ zigzag carbon nanotubes, n integer, suggest that the two lowest-lying phases are degenerate. Therefore, de-confined low-energy topological spin defects would occur. Then, these carbon nanotubes should be conductors, in analogy to polyacetylene. In clear contrast, no such degeneracy is obtained for either, $h = 3n + 1$ or $h = 3n$, so bound pairs of topological spin defects are expected to occur in these cases. Our findings provide further insights into electron correlation and exchange effects in carbon nanotubes.

PACS. 73.63.Fg Nanotubes – 75.10.Jm Quantized spin models – 71.27.+a Strongly correlated electron systems

1 Introduction

The first direct observation of carbon nanotubes (CNTs) was recorded in 1952 [1], while an image of a CNT was published in 1976 [2]. However, CNT did not become a worldwide research focus until the work of Iijima [3,4], and Wang and Buseck [5]. The one-dimensional (1D) character of CNTs immediately attracted a great scientific and technological interest [6,7]. For instance, they are a paradigmatic experimental realization of quantum wires. First, the 1D systems show remarkable physical properties, inducing a strongly correlated electronic state. Second, the miniaturization of electronics has continuously pushed the research into low-dimensional systems. The resulting transport properties can be most simply attributed to the 1D character. See Ref. [8] for a review.

CNTs have the form of rolled graphitic sheets with diameters ranging from a few nanometres to several hundred nanometres. Specifically, diameters for single-walled CNTs are on the order of 1 nm. Different CNTs can be identified by the *helicity* [7,9], a graphitic-sheet lattice vector corresponding to the lattice point to be superposed to the origin, $(N_1, N_2) \equiv N_1 \mathbf{a}_1 + N_2 \mathbf{a}_2$, where N_1 and N_2 are integers, and \mathbf{a}_1 and \mathbf{a}_2 define a set of primitive vectors of the graphitic lattice. See, for instance, Fig. 1(a).

We focus our attention on the zigzag $(h, 0)$ single-walled CNTs, with length $L = N_l \mathbf{a}_2$, where $N_l \rightarrow \infty$. For instance, CNTs with h hexagons around the tube. On the basis of band structure calculations it has been pre-

dicted [6,7] that $(h, 0)$ CNTs will be metallic when $h/3$ is an integer, and otherwise semiconductors. The rationalization of this behaviour is based on whether one of the sparse allowed values of the crystal momentum component in the \mathbf{b}_1 direction, $\mathbf{k}_1 = n\mathbf{b}_1/h$, can take the value $\mathbf{k}_1 \equiv \mathbf{b}_1/3$, so the graphitic-sheet crystal momentum on the vertex of the Brillouin zone, $\mathbf{k}_K = \mathbf{b}_1/3 + \mathbf{b}_2/2$, with zero-energy gap, exists (see Fig. 1(b)).

Here we address the problem from an alternative approach to the electronic structure of CNTs. It is known that electron correlation is important for carbon conjugated compounds [10–12]. Furthermore, it is well known that the (covalent-structure) valence-bond (VB) model or, equivalently, the Heisenberg Hamiltonian includes most of the electron correlation. Thence, early in 1984 [13] an effective valence-bond Hamiltonian of the Heisenberg type was extracted from ab initio extended basis set Configuration Interaction calculations on ethylene lowest electronic states. When the nanotube is formed by regular hexagons, up to a constant, this Hamiltonian can be written as

$$H = J \sum_{\langle mi, nj \rangle} \mathbf{S}_{mi} \cdot \mathbf{S}_{nj}, \quad (1)$$

where \mathbf{S}_{mi} is the spin operator for the spin on the carbon atom i of the polyene-ring-building-block m of the CNT, and $\langle mi, nj \rangle$ indicates that mi and nj are nearest neighbours. According to the Lieb and Mattis theorem [14] the ground state for the undoped half-filled bipartite system must be a singlet. Therefore, the appropriate ground-state wave function could have a resonating-

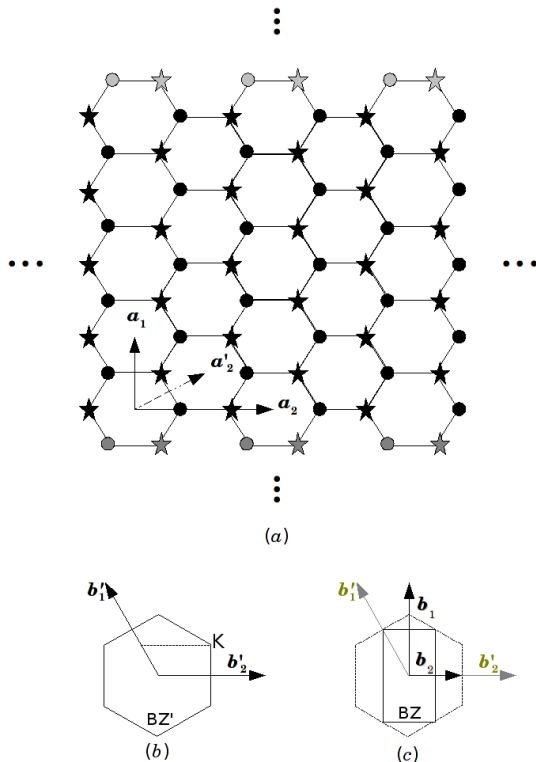


Fig. 1. (a) A fragment of a graphitic sheet showing the set of lattice primitive vectors, \mathbf{a}_1 and \mathbf{a}'_2 , and a translational-symmetry primitive vector along the direction of the CNT, \mathbf{a}_2 . (b) The corresponding Brillouin Zone of the graphitic lattice. (c) The Brillouin Zone for the zigzag carbon nanotube superposed to the Brillouin Zone of the graphitic lattice.

valence-bond (RVB) character. Long ago it was pointed out that RVB wave functions for linear Heisenberg chains exhibit long-range spin-pairing order (LRSPO) that allows to separate the set of (covalent) VB configurations in different subsets or phases [15]. Furthermore, a family of polymer strips were also argued to exhibit LRSPO [16–18]. Later, distortions in polyacetylene [19], polyacene [20], and a family of conjugated polymers [21], were investigated on the basis of LRSPO. Topological long-range order of RVB wave functions for the square lattice have also been investigated by different authors [22–25]. More recently, LRSPO for antiferromagnetic spin-1/2 has been generalized to hold for bipartite stripes [26–28]. Most of the considerations associated to the existence of this LRSPO for stripes are readily applicable to CNTs. Our goal is to elucidate when the ground state of different phases can be degenerate in analogy to what happens in polyacetylene.

This paper is organized as follows: In Sec. 2 we review the main LRSPO concepts [26–28]. In Sec. 3 the dimer-covering-counting approximation is reviewed and particularized to CNTs. Counting of the dimer-covering configura-

tions has been achieved by means of a transfer-matrix technique [26–28]. In Sec. 4 the energy per polyene-ring generating the CNT, with h ranging from 3 to 19, for the different LRSPO phases is analysed and discussed. Finally, a summary and the conclusions are given in Sec. 5.

2 Long-range spin-pairing order

From the Lieb and Mattis theorem [14] it is well known that for bipartite spin systems a *maximally-spin-paired* ground state is expected. In particular, at half filling, with equal number of sites in the \mathcal{A} and \mathcal{B} sublattices, the ground state is a singlet. Singlet states can be achieved by configuration interaction (CI) among covalent VB configurations or RVB. For instance, a linearly independent set of VB configurations can be obtained by pairing to a singlet each spin in the sublattice \mathcal{A} to a spin in the sublattice \mathcal{B} . The lowest lying VB singlets are the dimer-covering configurations where every spin in the sublattice \mathcal{A} is paired to one of its neighbours (see Fig. 2).

It is known [26–28] that any (covalent) VB configuration exhibits a LRSPO related to the local (at boundary) array of spin-pairings (SPs) penetrating any boundary f_m (see, for instance, Fig. 2). The parameter associated with the LRSPO, p , can take $h + 1$ different relevant values:

$$p = 0, 1, \dots, h. \quad (2)$$

This LRSPO allows to separate the set of VB configurations in different subsets or phases. Since two singlets from different phases must be different repeatedly at every position along the CNT, they are asymptotically orthogonal and non interacting via any interaction mediated by a few-particle operator. Then the matrix of the Hamiltonian asymptotically block-diagonalizes, so configurations belonging to different phases do not mix in the CI sense. Thus p may be taken as a long-range order parameter labeling the eigenstates of the p block.

Now, half-filled excited states or slightly doped states are analysed via topological spin defects (TSDs). There are different types of excitations conceivable from a *maximally-spin-paired* ground state. Let us say, preserving half filling (i.e., one electron per site), there are primarily spin excitations. In this case, two spin-wearing TSDs, one in the sublattice \mathcal{A} and the other in the sublattice \mathcal{B} , are obtained by breaking one SP to form a triplet state. Away from half-filling, there are low-energy spin and charge excitations. For instance, removing (adding) one electron produces two sites that cannot be SP, a charge-wearing TSD and a spin-wearing TSD, one in the sublattice \mathcal{A} and the other in the sublattice \mathcal{B} , the CNT becoming a doublet. In this case hopping terms must be retained in the Hamiltonian and the so-called t - J model or different extensions that incorporate either next-nearest-neighbour hopping t' or electrostatic repulsion have been employed so far. Thence, the doublet is a weighted superposition of VB configurations with a spin-wearing TSD and a charge-wearing TSD lying in different sublattices. Still, going up in the hierarchy of Hamiltonians, the Hubbard or even

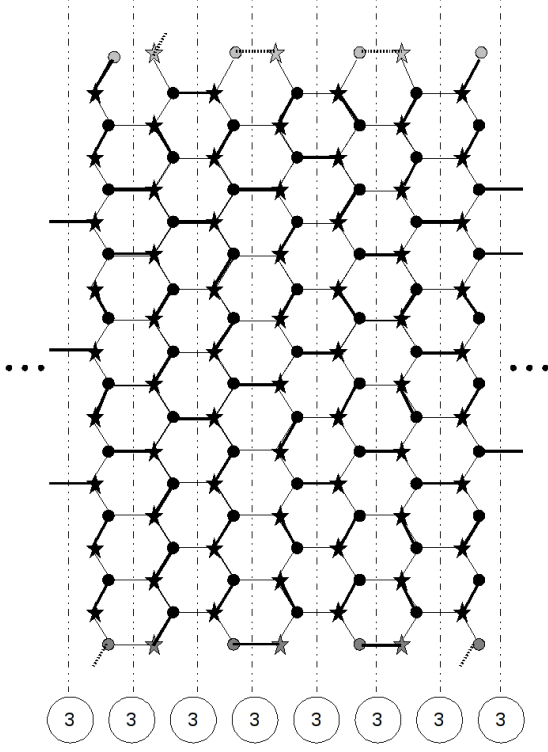


Fig. 2. A fragment of a VB configuration for a $h = 9$ CNT. Thick lines represent the spin-pairing (SP) to a singlet between a spin on a site in the sublattice \mathcal{A} (circles) with a spin on a site in the sublattice \mathcal{B} (stars). Gray circles and stars on the top correspond to the identical grey circles and stars at the bottom. Below each boundary, i.e. the two-dots-dash lines running midway two consecutive polyene-rings-building-blocks of the CNT, it appears the count of SPs, p , penetrating this boundary.

a more general Hamiltonian must be considered. In this case, still another type of excitations (though presumably of higher energy if a Heisenberg-type Hamiltonian is assumed to govern the lowest-lying region of the spectrum) can be produced relaxing the single-occupancy constrain. This leads to the *ionic* states, i.e., states with at least a pair of sites, one doubly occupied and the other empty, namely one negatively charge-wearing TSD and one positively charge-wearing TSD.

Of special relevance here is how the LRSPO is disrupted by a TSD (see Fig. 3). For instance, a TSD in a site $[m, i]$, m indicating the polyene-ring-building-block of the CNT and i the specific carbon in the ring, can be seen as a domain wall located on the polyene ring m , which separates the CNT in two sectors with associated left, p_l , and right, p_r , order parameters.

$$\begin{aligned} p_r &= p_l - 1, & i \in \mathcal{A}, \\ p_r &= p_l + 1, & i \in \mathcal{B}. \end{aligned} \quad (3)$$

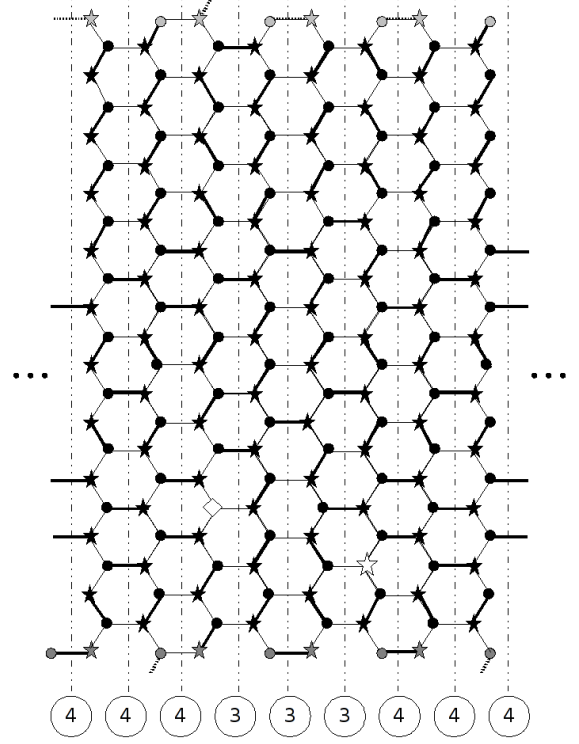


Fig. 3. A fragment of a VB configuration for a $h = 11$ CNT containing a pair of TSDs, one in the sublattice \mathcal{A} (white diamond) and the other in the sublattice \mathcal{B} (white star). Notice that this VB configuration shows LRSPO $p = 4$ everywhere but in the intervening region defined by the pair of TSDs, with $p = 3$.

Thence, to fulfil boundary conditions TSDs must appear by pairs, one TSD in the sublattice \mathcal{A} and the other in the sublattice \mathcal{B} , to ensure $\Delta p = 0$ from the left to the right of the pair. Such a pair define an intervening region with $\Delta p = \pm 1$ with respect to the LRSPO p of the host (see Fig. 3). If the energy per polyene ring associated to the intervening region is higher than the energy per polyene ring associated to the host, the pair of TSDs should try to remain as close as possible. Thence, bound pairs of TSDs would exist. Otherwise, if the energy per ring associated to the intervening region is degenerate with the energy per ring associated to the host, the pair of TSDs can be deconfined. To show that this is the trend for some values of h is one of the concerns of the present paper.

3 Dimer-covering counting approximation

Within the *dimer-covering-counting* approximation the *resonance energy*, $E_r(h, p)$ in units of J , i.e., the energy correction below the energy of a single dimer-covering structure, depends on the CI among the different dimer-covering

configurations with LRSP0 p . When an equally weighted wave function is considered, it has been argued [16, 29, 30] that one might consider this energy lowering to depend solely on the dimension of the space spanned by the appropriate dimer-covering configurations. Let $\mathcal{N}_p(h)$ be the number of linearly independent dimer-covering configurations with the LRSP0 p . Since $\mathcal{N}_p(h)$ is multiplicative in terms of a break up into subsystems while the energy is additive, such a functional dependence should be of the form

$$E_r(h, p) \approx -C \ln \mathcal{N}_p(h), \quad (4)$$

C is a fitting parameter independent of the structure to some degree. For the nearest-neighbour isotropic Heisenberg model of a class of benzenoid hydrocarbons [16] it has been obtained $C = 0.5667$ by fitting the logarithm of the dimer-covering count to the resonance energy calculated from an equally weighted dimer-covering wave function.

A variety of different enumeration methods have been developed for dimer coverings [31]. Here, the values $\mathcal{N}_p(h)$ for a maximally spin-paired half-filled system can be easily obtained by a transfer-matrix technique [26–28]. Let us analyse from a local point of view the dimer-covering singlets. We can identify the dimer-covering local states according to which carbon atoms show a pairing across the f_m boundary. In the present case it can be seen that, for each boundary, there are 2^h different local states, $|e_{mI}\rangle$ (I ranging), which can be classified according to the value of p , $|e_{mI}^p\rangle$, in different subsets of dimension

$$D_{h,p} = \frac{h!}{p!(N-p)!}. \quad (5)$$

For each value of h and p , proceeding from the left to the right, from the boundary f_{m-1} to boundary f_m , a dimer-covering-counting matrix, \mathcal{K}_m , where the matrix elements, $(e_{m-1I}|\mathcal{K}_m|e_{mJ})$, are the number of different ways $|e_{mJ}\rangle$ can succeed $|e_{m-1I}\rangle$. Then, the number of dimer-covering states in a p subspace is

$$\mathcal{N}_p(h) = \sum_{e_I^p} (e_I^p|\mathcal{K}_1\mathcal{K}_2 \cdots \mathcal{K}_{2N_I}|e_I^p). \quad (6)$$

It is easy to see that $\mathcal{K}_{m+1} \equiv \mathcal{K}_m^*$, where \mathcal{K}_m^* is the transposed of \mathcal{K}_m . Therefore, $T_m \equiv \mathcal{K}_m\mathcal{K}_m^*$ is a block-diagonal symmetric matrix that does not depend on m , so we can omit this sub-index. For $L \rightarrow \infty$, the highest eigenvalue $\Lambda_{(h,p)}$ of the p block, T_p , dominates, and

$$\mathcal{N}_p(h) \approx \Lambda_{(h,p)}^{N_I}. \quad (7)$$

Then, the Heisenberg energy, in units of J , as a function of h and p of the CNT is

$$\begin{aligned} E_p(h) &\approx 4hN_I\varepsilon_0 + E_r(h, p) \\ &\approx 4hN_I\varepsilon_0 - CN_I \ln \Lambda_{(h,p)}, \end{aligned} \quad (8)$$

where $\varepsilon_0 = -0.3750$ is the energy per site in units of J of a single dimer-covering configuration. From Eq. 8 we can obtain the Heisenberg energy per carbon atom,

$$\varepsilon_p(h) \approx \varepsilon_0 - C \frac{1}{2h} \ln \Lambda_{(h,p)}, \quad (9)$$

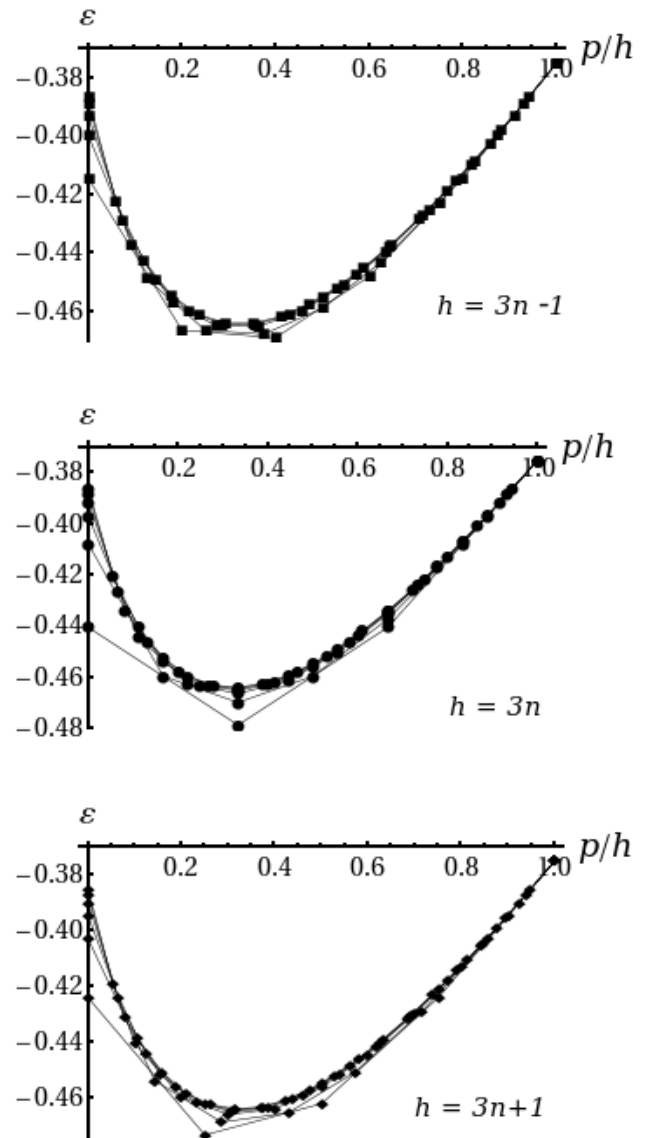


Fig. 4. The energy per carbon atom as a function of p/h . From top to bottom: $h = 3n - 1$ (■), $h = 3n$ (●), $h = 3n + 1$ (◆), with $n = \text{integer}$ and h decreasing from top to bottom.

where $\lambda_{(h,p)} = \Lambda_{(h,p)}^{1/2}$. However, for CNT, due to the quasi-1D character, it is relevant the Heisenberg energy per polyene-ring unit of the CNT,

$$\mathcal{E}_p(h) \approx 2h\varepsilon_0 - C \ln \lambda_{(h,p)}. \quad (10)$$

4 Results and discussion

We have computed the values of $\lambda_{(h,p)}$ for $h = 3, 4, \dots, 19$ and $p = 0, 1, 2, \dots, h$. Since nearest-neighbour separation of graphitic systems is $d_{C-C} \approx 0.142$ nm, these values of h include realistic CNTs with diameters ranging from 0.5 nm to 1.5 nm which correspond to $h \approx 6$ and $h \approx 19$, respectively. From the values of $\lambda_{(h,p)}$, the energies per carbon atom, $\varepsilon_p(h)$, in units of J , are readily obtained

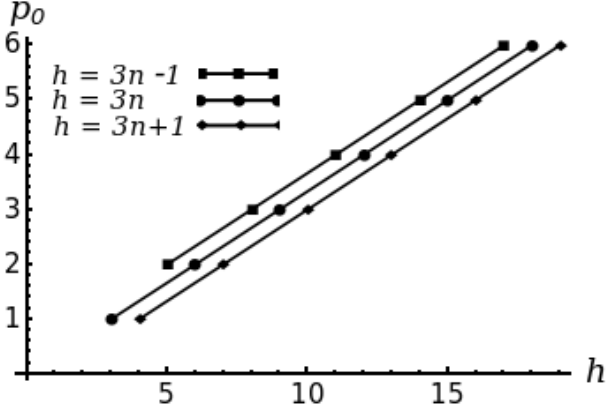


Fig. 5. The value of the phase p_0 yielding the lowest-lying energy per polyene ring, for $h = 3n$ (\bullet), $h = 3n + 1$ (\blacklozenge), and $h = 3n - 1$ (\blacksquare).

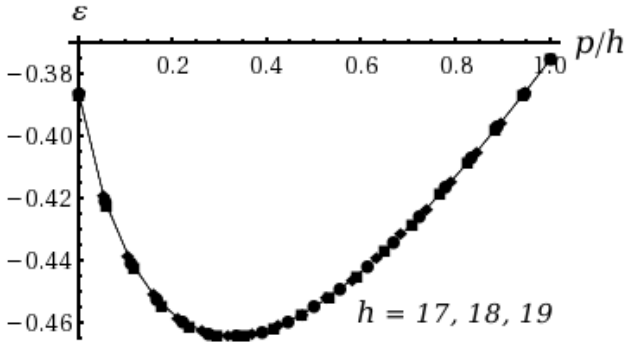


Fig. 6. The energy per carbon atom for $h = 17, 18, 19$.

using Eq. (9). In Fig. 4 these energies are represented as a function of p/h . We observe that the energy per carbon atom as a function of p/h behaves differently according to h being equal to $3n - 1$, $3n$ or $3n + 1$. First, the ground-state energy per carbon atom is obtained when the phase, which we design as p_0 , is the integer closest to $h/3$, as shown in Fig. 5. And second, the values of the energy per carbon atom of the two lowest-lying phases suggest that degeneracy may occur when $(h + 1)/3$ is an integer. Nevertheless, with increasing values of h , the energies per carbon atom as a function of p/h for $h = 3n - 1, 3n, 3n + 1$ tend to converge to the same function, with the energies of the lowest-lying phases converging to a common value, as expected for an infinite graphitic sheet. See, for instance, Fig. 6.

Restricting ourselves to finite h , for the sake of analyzing whether the pairs of topological spin defects should remain confined or not, it is worthwhile to compare the energy per polyene ring of the different phases, instead the energies per carbon atom. Therefore, we have computed the difference in energy per polyene ring, $\Delta(h)$, in units

of J , between the two lowest-lying phases, p_0 and p_1 ,

$$\Delta(h) \approx C \ln \frac{\lambda_0}{\lambda_1}. \quad (11)$$

From the values of $\Delta(h)$ it is noted that degeneracy between the two lowest-lying phases occurs when $(h + 1)/3$ is an integer. See, for instance, Fig. 7, where $\Delta(h)$ is represented as a function of h for $h = 3n - 1, 3n, 3n + 1$. Therefore, the pair of TSDs can be deconfined when $h = 3n - 1$. On the contrary, for $(h - 1)/3$ and $h/3 = \text{integer}$ the energy per polyene ring for phases other than p_0 are higher, so the energy per polyene ring associated to the intervening region is higher than the energy of the host belonging to the p_0 phase. Thence, for $h = 3n$ and $h = 3n + 1$ the pair of TSDs should be confined and bound pairs of TSDs would exist.

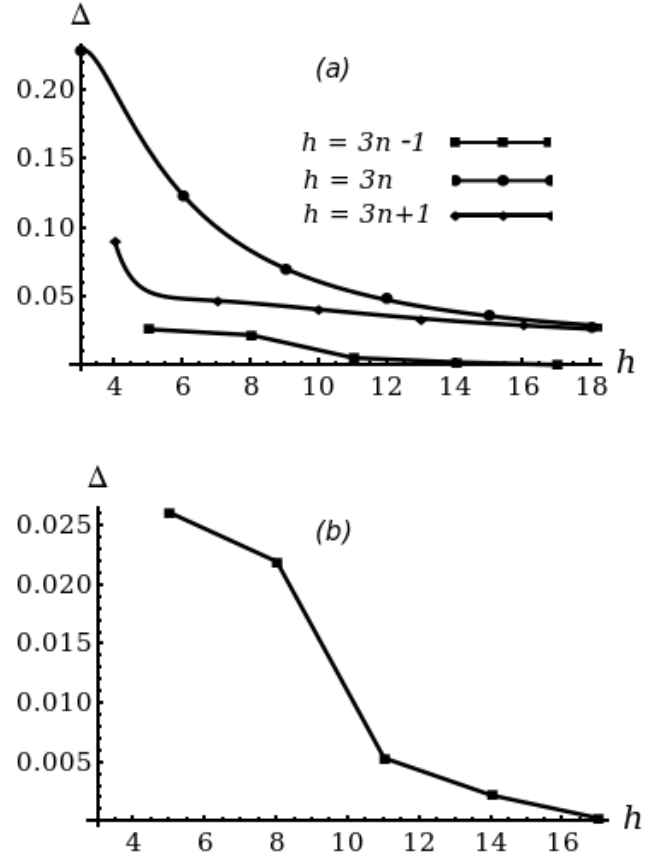


Fig. 7. (a) Difference in energy, $\Delta(h)$, per polyene ring, in units of J between the two lowest-lying phases, p_0 and p_1 , as a function of the number of hexagons around the CNT. De continuous lines, from top to bottom, correspond to $h = 3n$ (\bullet), $h = 3n + 1$ (\blacklozenge), and $h = 3n - 1$ (\blacksquare), respectively. The top two continuous lines are obtained by fitting the Δ values by a power series on $1/h$, and tend asymptotically to 0.0125907 and 0.0123187, respectively. The bottom continuous line is obtained by simply joining the calculated values of Δ . (b) Δ for $h = 3n - 1$, for $n = 2, \dots, 6$.

The analysis the eigenvectors can help to understand this behaviour. We note that the highest-weighted components of the eigenvectors for $h/3 = \text{integer}$, are those with the $p_0 = h/3$ bonds of the local VB configurations distributed at a ratio of *one of every three*. The weight of the components of the eigenvectors decreases when the number of bonds on the local VB configuration becomes closer than *one of every three* (see, for instance, Fig. 8). This tendency is maintained for higher values of h . For

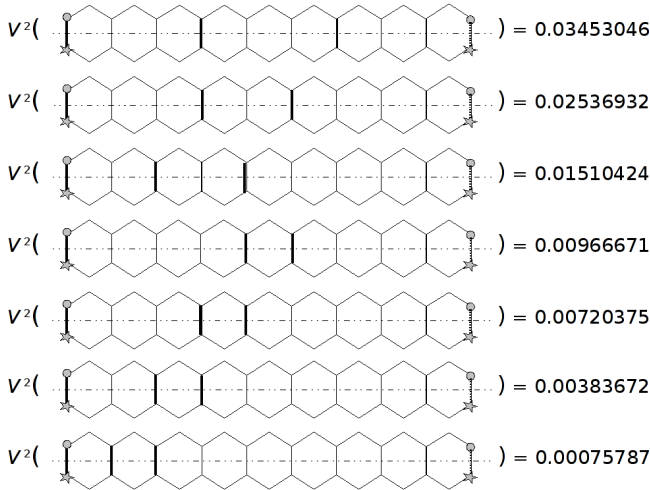


Fig. 8. Some representative values of the weight of different local VB configurations for $h = 9$ and $p_0 = 3$.

instance, when going up to $h = 18$ the weight of a VB configuration with the $p_0 = 6$ bonds equally-distributed is ≈ 497.9 times the weight of a VB configuration with all the bonds as close as possible. The exact uniform distribution of *one of every three* bonds can not be fulfilled when $h = 3n \pm 1$, $n = \text{integer}$. When this happens, $p_0 = (h \mp 1)/3$ and $p_1 = (h \pm 2)/3$. For $p_0 = (h + 1)/3$ local VB configurations show at least a pair of bonds being closer than *one of every three*, so the energy is not substantially lowered with respect to the energy of the p_1 that allows local VB configurations with not so close bonds.

A full analysis of the available experimental results under the optics of the present work is a hard task. As far as I know, most CNTs are not fabricated; instead, they self assemble, and helicity is not controlled. Furthermore, as-prepared single-walled CNTs generally contain a mixture of metallic and semiconducting species in a ratio of $\sim 1/3$ and $\sim 2/3$, respectively. In addition, most of the experimental work is based on chiral CNTs [32], different species of nanotubes being distinguished by their optical fingerprints [33,34] or scanning tunnelling microscopy [9, 35]. However, common trends can be envisaged. In this regard, it is noteworthy that Δ is decreasing as $\sim 1/h$ for most of the CNTs, as expected [9,33,35], since Δ is somehow related with the transition energy. In addition, it is also remarkable that the existence of different non-interacting dimer-covering VB phases which could(not) be

degenerated, is compatible with the existence of observed non-local effects [36].

5 Summary and conclusions

We have obtained the Heisenberg energy per carbon atom, and also per polyene ring in units of J for zigzag single-walled CNTs, with the number of hexagons around the CNT, h , ranging from 3 to 19, and LRSPO phases p ranging from zero to h . We found that the phase p_0 that yield the ground state is the closest integer to $h/3$. From the energy difference per polyene ring between the two lowest-lying phases, p_1 and p_0 , we conclude that degeneracy is expected for $h = 3n - 1$, so TSD should be deconfined, in analogy to polyacetylene. On the contrary, for $h = 3n$ and $h = 3n + 1$ the gap between the two lowest-lying phases tend asymptotically to a non-zero value, so the pair of TSDs should be confined and bound pairs of TSDs are expected to occur. These findings provide further insights into electron correlation and exchange effects in carbon nanotubes.

Acknowledgement

The largest calculations described in this work where performed at the Institut de Química Teòrica i Computacional (IQTC-UB).

References

1. L. V. Radushkevich and V. M. Lukyanovich, *Zum. Fisic. Chim.* **26**, 88 (1952).
2. A. Oberlin, M. Endo, and T. Koyama, *J. Cryst. Growth* **32**, 335 (1976).
3. S. Iijima, *Nature* **354**, 56 (1991).
4. S. Iijima and T. Ishihashi, *Nature* **363**, 603 (1993).
5. S. Wang and P.R. Buseck, *Chem. Phys. Lett.* **182**, 1 (1991).
6. J. W. Mintmire, B. I. Dunlap, and C.T. White, *Phys. Rev. Lett.* **68**, 631 (1992).
7. N. Hamada, S.I. Sawada, and A. Oshiyama, *Phys. Rev. Lett.* **68**, 1579 (1992).
8. J.-C. Charlier, X. Blase, and S. Roche, *Rev. Mod. Phys.* **79**, 677 (2007).
9. T. W. Odom, J.-L. Huang, P. Kim, and C. M. Lieber, *Nature* **391**, 62 (1998).
10. B. Hudson and B.E. Kohler, *J. Chem. Phys.* **59**, 4984 (1973).
11. I.R. Ducasse, T.E. Miller, and Z.G. Soos, *J. Chem. Phys.* **76**, 4094 (1982).
12. Z.G. Soos and S. Ramasesha, *Chem. Phys. Lett.* **101**, 34 (1983).
13. M. Said, D. Maynau, J.-P. Malrieu, and M.A. Garcia-Bach, *J. Am. Chem. Soc.* **106**, 571 (1998).
14. E.H. Lieb and D.C. Mattis, *J. Math. Phys.* **3**, 749 (1962).
15. D.J. Klein and M.A. Garcia-Bach, *Phys. Rev. B* **19**, 877 (1979).

16. W.A. Seitz, D.J. Klein, T.G. Schmalz, and M.A. Garcia-Bach, Chem. Phys. Lett. **115**, 139 (1985); **118**, 110E (1985).
17. D.J. Klein, T.G. Schmalz, G.E. Hite, A. Metropoulos, W.A. Seitz, Chem. Phys. Lett. **120**, 367 (1985).
18. G.E. Hite, A. Metropoulos, D.J. Klein, T.G. Schmalz, W.A. Seitz, Theor. Chim. Acta **69**, 369 (1986); D.J. Klein, G.E. Hite, W.A. Seitz, T.G. Schmalz, *ibid*, p. 367 (1986).
19. M.A. Garcia-Bach, P. Blaise, and J.-P. Malrieu, Phys. Rev. B **46**, 15645 (1992).
20. M.A. Garcia-Bach, A. Peñaranda, and D.J. Klein, Phys. Rev. B **45**, 10891 (1992).
21. M. A. Garcia-Bach, R. Valentí, and D. J. Klein, Phys. Rev. B **56**, 1751 (1997).
22. S.A. Kivelson, D.S. Rokhsar, and J.P. Sethna, Phys. Rev. B **35**, 8865 (1987).
23. S. Kivelson, Phys. Rev. B **36**, 7237 (1987).
24. D.J. Klein, T.G. Schmalz, M.A. Garcia-Bach, R. Valentí, and T.P. Živković, Phys. Rev. B **43**, 719 (1991).
25. D.J. Klein, T. P. Živković, and R. Valentí, Phys. Rev. B **43**, 723 (1991).
26. M.A. Garcia-Bach, Eur. Phys. J. B **14**, 439 (2000).
27. M.A. Garcia-Bach, "Many-body VB ansätze. From polymers and ladder materials to the square lattice", *Valence Bond Theory*, (Elsevier, New York, 2002), pp. 729-768.
28. M.A. Garcia-Bach, Phys. Rev. B **72**, 024530 (2005).
29. D.J. Klein, G. E. Hite, and T. G. Schmalz, J. Comput. Chem. **7**, 443 (1986).
30. T.P. Živković, B.L. Sandleback, T.G. Schmalz, and D.J. Klein, Phys. Rev. B **41**, 2249 (1990).
31. D.J. Klein, G.E. Hite, W.A. Seitz, T.G. Schmalz, Theor. Chim. Acta **69**, 409 (1986).
32. R. Matsunaga, K. Matsuda, and Y. Kanemitsu, Phys. Rev. Lett. **106**, 037404 (2011), and references therein.
33. M. S. Strano, J. Amer. Chem. Soc. **125**, 16148, (2003).
34. M. S. Dresselhaus, G. Dresselhaus, and A. Jorio, J. Phys. Chem. C **111**, 17887 (2007), and references therein.
35. J. W. G. Wildöer, L. C. Venema, A. G. Rinzler, R. E. Smalley, and C. Dekker, Nature **391**, 59 (1998).
36. L. G. Herrmann, F. Portier, P. Roche, A. Levy Yeyati, T. Kontos, and C. Strunk, Phys. Rev. Lett. **104**, 026801 (2010). See also Viewpoint: N. Mason, Phys. **3**, 3 (2010).